Monthly Notices of the ROYAL ASTRONOMICAL SOCIETY
MNRAS **457,** 3178–3190 (2016) doi:10.1093/mnras/stw195

Broad-band linear polarization in late-type active dwarfs

Manoj K. Patel,[1⋆] Jeewan C. Pandey,[2⋆] Subhajeet Karmakar,[2⋆] D. C. Srivastava[1] and Igor S. Savanov[3]

[1]*Department of Physics, Deen Dayal Upadhyay Gorakhpur University, Gorakhpur-273009, India*
[2]*Aryabhatta Research Institute of Observational Sciences (ARIES), Nainital-263 001, India*
[3]*Institute of Astronomy, Russian Academy of Sciences, ul. Pyatnitskaya 48, Moscow, 119017, Russia*

Accepted 2016 January 20. Received 2015 December 23; in original form 2015 November 11

ABSTRACT

We present recent polarimetric results of magnetically active late-type dwarfs. The polarization in these stars is found to be wavelength dependent, decreasing towards the longer wavelength. The average values of degree of polarization in these active dwarfs are found to be 0.16 ± 0.01, 0.080 ± 0.006, 0.056 ± 0.004 and 0.042 ± 0.003 per cent in *B*, *V*, *R*, and *I* bands, respectively. Present results indicate that polarization in the majority of active dwarfs are primarily due to sum of the polarization by magnetic intensification and scattering. However, supplementary sources of the polarization are also found to be present in some active stars. The correlations between the degree of polarization and various activity parameters like Rossby number, chromospheric activity indicator and coronal activity indicator are found to be stronger in *B* band and weaker in *I* band.

Key words: techniques: polarimetric – stars: activity – stars: late-type – stars: magnetic field – starspots.

1 INTRODUCTION

The inhomogeneity due to the magnetic areas (star spots or plages) and circumstellar gas or dust envelopes on the surface of magnetically active late-type dwarfs may produce a broad-band linear polarization (BLP; Tinbergen & Zwaan 1981). The polarization of the integrated stellar light may change along with the stellar activity phenomenon (Huovelin, Saar & Tuominen 1988; Huovelin et al. 1989). The connection of magnetic field regions with BLP was first shown by Dollfus (1958) and Leroy (1962), and observed by Piirola (1977). The sources of linear polarization in late-type active dwarfs are still unclear. However, the most popular mechanisms those have been suggested by many studies are magnetic intensification and scattering due to circumstellar material. The BLP in cool active stars increases towards shorter wavelengths. Such wavelength-dependent polarization also supports the models for magnetic and scattering origins of polarization (Huovelin et al. 1985; Leroy & Le Borgne 1989). The number of saturated magnetically sensitive absorption lines increases towards shorter wavelengths and represents the characteristic of the observed wavelength-dependence polarization (Kemp & Wolstencroft 1974; Calamai, Landi Degl'Innocenti & Landi Degl'Innocenti 1975; Tinbergen & Zwaan 1981). But a similar effect could be produced by Rayleigh scattering in the optically thin part of the stellar atmosphere. Magnetic intensification in the saturated Zeeman sensitive lines will arise from stellar spots and plages (Leroy 1962; Mullan & Bell 1976; Huovelin & Saar 1991; Saar & Huovelin 1993), while the scattering could take place in optically thin discs or other inhomogeneities above the stellar surface (Brown & McLean 1977; Brown, McLean & Emslie 1978; Pfeiffer 1979; Piirola & Vilhu 1982).

Measurements of BLP have been made for numerous late-type active dwarfs in the past. Huovelin et al. (1985) have made polarimetric studies in *U*, *B*, *V*, *R*, and *I* bands of a sample of 13 solar-type stars and have found that the intrinsic polarization decreases towards longer wavelengths only for the stars HD 20630, HD 20998, HD 126053, and HD 206860. Leroy & Le Borgne (1989) conducted a survey of 30 solar-type stars and found no evidence of intrinsic polarization. Apart from these surveys, many other solar-type stars are observed polarimetrically and the polarization is explained either by magnetic origin or scattering of thin circumstellar material or sum of both. Some studies show that the degree of linear polarization depends on the photospheric, chromospheric, and coronal activity levels of the star and follows the short period changes in activity caused by rotational modulation, suggesting a magnetic origin (see Tinbergen & Zwaan 1981; Huovelin et al. 1988, 1989; Alekseev 2000, 2003).

Evidence for a connection between linear polarization and magnetic activity indicators is lacking because on one hand the variation, as well as the mean degree of polarization of late-type dwarfs are very small, and on the other hand sizes of samples studied are small. Therefore, we have observed a sample of 50 active late-type dwarfs and supplemented it with another sample of 18 active dwarfs, those are available in the literature (Huovelin et al. 1985; Alekseev 2000, 2003; Golovin et al. 2012; Patel et al. 2013). The criteria of

⋆ E-mail: patelmanoj79@gmail.com (MKJ); jeewan@aries.res.in (JCP); subhajeet@aries.res.in (SK)

selection of stars in the sample were (i) the *V*-band magnitude range of 6.0–12.0 mag, and (ii) the $(B - V)$ colour range of 0.5–1.5 mag. Since these late-type active stars exhibit very small value of polarization, therefore, the fainter limit was set as 12 mag for our polarimeter. Going fainter than this show large error bars due to photon statistics. The upper limit of 6.0 mag is because of the fact that as going brighter than this limit the CCD saturates even in a small exposure. Basic parameters of these stars are summarized in Table 1.

The paper is organized as follows. We describe observations and data reduction in the next section, while analysis and results are given in Section 3. In Section 4, we provide the correlation of linear polarization with activity parameters, and in the last section, we present discussion and conclusions.

2 OBSERVATIONS AND DATA REDUCTION

Polarimetric observations of stars in the sample were obtained during the years 2010–2014 using ARIES Imaging Polarimeter (AIMPOL; Rautela, Joshi & Pandey 2004) mounted at the Cassegrain focus of the 104 cm Sampurnanand telescope of the Aryabhatta Research Institute of Observational Sciences, Nainital, India, coupled with a 1024 × 1024 CCD camera. AIMPOL consists of a half-wave plate (HWP) modulator and a Wollaston prism beam-splitter. Each pixel of the CCD corresponds to 1.73 arcsec and the field of view is ∼ 8 arcmin in diameter. The read-out noise and the gain of the CCD are 7.0e^- and 11.98e^- ADU^{-1}, respectively. For linear polarimetry, HWP is rotated with an interval of 22.°5 between exposures. Thus, one polarization measurement was obtained from every four exposures at the HWP position of 0°, 22.°5, 45° and 67.°5. The exposure time at each position of the HWP was same; ranging from 5 to 300 s depending on the filter used. The full width at half-maximum of the stellar image varied from 2 to 3 pixels. Due to the absence of a grid in AIMPOL, we manually checked for any overlap of ordinary and extraordinary images of the sources.

Fluxes of ordinary (I_o) and extraordinary (I_e) beams for all the observed sources with a good signal-to-noise ratio were extracted by standard aperture photometry after bias subtraction using the IRAF[1] package. We have calculated the ratio R(α) as

$$R(\alpha) = \frac{I_e(\alpha) - I_o(\alpha)}{I_e(\alpha) + I_o(\alpha)} = P\cos(2\theta - 4\alpha), \quad (1)$$

where P is the fraction of the total linearly polarized light and θ is the polarization angle of the plane of polarization. Here, α is the position of the fast axis of the HWP at 0°, 22.°5, 45° and 67.°5 corresponding to the four normalized Stokes parameters, respectively, $q[R(0^\circ)]$, $u[R(22.^\circ5)]$, $q_1[R(45^\circ)]$ and $u_1[R(67.^\circ5)]$. The detailed descriptions about the AIMPOL, data reduction, calculations of polarization, and position angle are given in Rautela et al. (2004).

In order to correct the measurements for null polarization (or instrumental polarization) and the zero-point polarization angle, we observed several polarized and unpolarized standard stars in each night of observations. Stars HD 236633, HD 204827, HD 19820, HD 25443, HD 154445, and BD+59° 389 were observed as standard polarized stars, while stars β UMa, θ UMa, HD 14069, BD+33° 2642, and GD 319 were observed as standard unpolarized stars. The observed degree of polarization [P (per cent)] and polarization angle [$\theta(^\circ)$] for the polarized standards are similar to the standard values as given by Schmidt, Elston & Lupie (1992). These measurements show that the instrumental polarization of Sampurnanand telescope is below 0.1 per cent in all passbands, which was found to be constant over the past few years (see Soam, Maheswar & Eswaraiah 2014). The instrumental polarization was then applied to all measurements. The values of degree of polarization and polarization position angle of active dwarfs as observed at different epochs are given in Table 2. The data of seven stars were of bad quality due to poor sky conditions. Therefore, our final sample consists only 43 stars.

[1] iraf.net

3 ANALYSIS AND RESULTS

The distributions of linear polarization of active dwarfs in *B*, *V*, *R*, and *I* bands are shown in Fig. 1. The mean value of polarization in *B* band was found to be 0.16 ± 0.01 per cent, which was more than that observed in other bands. The average values of degree of linear polarization in *V*, *R*, and *I* bands are found to be 0.080 ± 0.006, 0.056 ± 0.004 and 0.042 ± 0.003 per cent, respectively.

3.1 Polarization due to interstellar medium (ISM)

The majority of stars in our sample are nearby and suffer negligible reddening. Therefore, it is natural to suppose that polarization due to ISM may be negligible. However, three stars namely V526 Aur, V1658 Aql and V1659 Aql are located at a distance more than 300 pc and may have suffered considerable reddening indicating that observed polarization may be due to the foreground ISM. Fig. 2 shows the plot between normalized Stokes parameters Q and U. The values of normalized Stokes parameters are concentrated near the origin (0,0) of the Q–U graph. However, the stars V526 Aur, V1658 Aql and V1659 Aql denoted by squares are located away from the origin indicating external sources of polarization. Further, in order to explore possibilities of ISM polarization, the average values of polarization are fitted to the standard Serkowski's polarization law (Serkowski, Mathewson & Ford 1975):

$$P_\lambda = P_{\max}\exp[-Kln^2(\lambda_{\max}/\lambda)], \quad (2)$$

where P_λ is the percentage polarization at wavelength λ and $P_{\max}$ is the peak polarization, occurring at wavelength $\lambda_{\max}$. Fig. 3 shows the best fit for Serkowski's polarization law to our BLP data for V526 Aur, V1658 Aql, and V1659 Aql. Adopting the parameter $K = 1.15$ (Serkowski 1973), if the polarization is well represented by the Serkowski relation, σ_1 (the unit weight error of the fit) should not be higher than 1.6 due to the weighting scheme; a higher value could be indicative of the presence of intrinsic polarization (see also Medhi et al. 2010; Eswaraiah et al. 2011). The best-fitting values of σ_1 are found to be 0.893, 0.508, and 0.445 for V526 Aur, V1658 Aql, and V1659 Aql, respectively, which indicate that observed values of linear polarization are due to the ISM. The best-fitting values of $P_{\max}$ and $\lambda_{\max}$ are found to be 0.57 ± 0.02, 0.57 ± 0.04 and 0.57 ± 0.01 (in per cent) and 0.50 ± 0.05, 0.53 ± 0.07 and 0.53 ± 0.04 (in μm) for V526 Aur, V1658 Aql, and V1659 Aql, respectively. The value of $\lambda_{\max}$ gives a clue about the origin of polarization. Stars with $\lambda_{\max}$ lower than the average value of the ISM (0.55 ± 0.04 µm; Serkowski et al. 1975) are probable candidates to have an intrinsic component of polarization (Orsatti, Vega & Marraco 1998). The determined values of $\lambda_{\max}$ are very close to the general ISM indicating that these stars have an extrinsic component of polarization. Using the relation $R_V = 5.6 \times \lambda_{max}$ (Whittet & Van Breda 1978), the total-to-selective extinction (R_V) are found to be 2.8 ± 0.3, 3.0 ± 0.4, and 2.9 ± 0.2 for V526 Aur, V1658 Aql, and V1659 Aql, respectively. These values of R_V are in

Table 1. Basic parameters of the stars in the sample.

S.No	Object	Sp. type	V (mag)	$(B-V)$ Mag	Period (d)	D (pc)	$\log(R_0)^\star$	$\log(R_X)^\star$	$\log(R'_{HK})^\star$
				Present observed sample					
1	PW And	K2V	8.852	0.936	01.76	032.40	− 1.103	− 3.232	...
2	BK Psc	K5V	10.57	1.160	02.16	035.92	− 1.049	− 3.000	...
3	BD −04 234	G0V	9.961	0.550	...	...	...	...	...
4	V1221 Tau	G6V/K3V	9.490	0.533	00.55	121.01	− 1.010	− 4.005	...
5	V988 Tau	K2V	9.370	0.950	09.90	060.14	− 0.357	− 4.632	− 4.394
6	V526 Aur	G0V	10.83	0.601	02.85	...	...	...	...
7	V538 Aur	K0V	6.210	0.840	11.00	012.28	− 0.273	− 4.742	− 4.254
8	V848 Mon	K2V	8.950	0.960	19.98	030.94	− 0.054	− 3.820	− 4.419
9	V850 Mon	K3V	9.310	0.940	09.90	054.27	− 0.355	...	− 4.313
10	V429 Gem	K5V	9.930	1.150	02.78	030.00	− 0.939	− 3.420	− 4.047
11	V867 Mon	K2V	8.144	0.883	04.76	024.53	− 0.656	− 4.531	− 4.218
12	BD+231799	K0V	9.980	1.090	20.03	034.40	− 0.376	− 2.855	...
13	HO Cnc	K5V	9.508	1.022	05.21	043.86	− 0.648	...	− 4.257
14	HP Cnc	K0V	9.060	0.746	11.14	030.76	− 0.367	− 3.999	− 3.480
15	V402 Hya	K0/K1V	8.980	0.770	00.41	031.16	− 0.900	− 3.050	...
16	V405 Hya	K2V	8.760	0.990	08.64	028.28	− 0.423	− 4.697	− 4.190
17	GT Leo	K0V	8.881	0.902	10.92	049.13	− 0.303	...	− 4.390
18	V417 Hya	K2V	8.124	0.913	10.74	024.02	− 0.313	− 5.084	− 4.199
19	LR Hya	K1.5V	8.020	0.855	06.87	034.22	− 0.485	− 4.746	− 4.190
20	V418 Hya	K2V	8.750	0.850	...	032.21	...	− 5.066	− 4.249
21	AB Crt	K3V	9.040	0.990	10.33	029.14	− 0.346	...	− 4.333
22	HL Leo	G2V	7.400	0.850	37.17	222.94	0.250	− 4.095	− 3.977
23	GQ Leo	K5Ve	10.90	1.020	04.45	050.00	− 0.717	− 2.897	...
24	PQ Vir	K0V	9.130	0.890	...	047.94	...	...	− 4.208
25	MY Uma	K0V	9.570	0.990	11.43	045.49	− 0.302	...	− 4.300
26	PR Vir	K3V	9.490	0.950	17.16	041.46	− 0.118	...	− 4.303
27	FZ Leo	G5V	8.430	0.560	00.91	102.07	− 0.880	− 3.253	...
28	LV Com	K2V	9.160	0.930	05.50	040.69	− 0.609	...	− 4.433
29	DO CVn	K0V	8.540	0.960	08.37	026.95	− 0.432	− 4.083	− 4.219
30	LX Com	K1V	9.100	0.890	07.74	037.47	− 0.448	− 4.603	− 4.151
31	PX Vir	K1V	7.690	0.847	06.47	021.68	− 0.507	− 4.288	− 4.108
32	GY Boo	K0V	8.900	0.970	09.52	033.25	− 0.378	− 4.081	− 4.233
33	GZ Boo	K2V	8.870	0.900	07.52	042.32	− 0.464	− 4.559	− 4.203
34	HO Boo	K2V	7.960	0.850	93.00	025.15	0.649	− 4.858	− 4.341
35	FN Boo	K6V	8.090	1.430	79.82	030.43	− 1.400	...	...
36	V1022 Her	K7V	11.71	1.504	00.81	030.00	− 1.525	− 2.950	...
37	V1658 Aql	K0V	9.350	1.110	18.76	409.00	...	− 2.930	...
38	V1659 Aql	K0V	8.870	1.080	05.18	339.00	...	...	...
39	V401 Vul	K3V	10.83	1.030	02.16	064.03	− 1.033	− 3.045	...
40	V402 Peg	K2V	7.730	0.911	04.51	019.75	− 0.690	− 5.416	− 4.606
41	OT Peg	K0V	9.740	0.810	...	074.04	...	− 3.065	...
42	V383 Lac	K1V	8.580	0.840	02.47	034.00	− 0.921	− 3.155	− 3.773
43	HD 218782	K2V	9.870	0.890	00.92	...	− 1.373	− 3.110	
				The sample taken from literature					
44	HD 1835	G3V	06.38	0.670	07.70	20.86	− 0.213	− 4.622	− 4.263
45	HD 20630	G5V	04.85	0.660	09.40	09.14	− 0.164	− 4.659	− 4.208
46	HD 25998	F7V	05.50	0.470	02.60	20.99	− 0.027	− 4.430	− 4.255
47	V1147 Tau	K5V	11.07	1.220	01.49	45.07	− 1.229	− 2.980	...
48	FR Cnc	K5V	10.24	1.110	00.83	34.07	− 1.460	− 3.289	− 3.480
49	LQ Hya	K0V	07.83	0.920	01.70	18.62	− 1.116	− 3.081	− 3.728
50	HD 114378	F5V	05.22	0.450	03.02	17.82	0.087	− 4.963	− 5.216
51	HD 114710	G0V	04.25	0.580	12.35	09.13	0.204	− 5.702	− 4.597
52	HD 115383	G0V	05.22	0.590	03.33	17.56	− 0.391	− 4.451	− 4.219
53	HD 126053	G1V	06.30	0.600	21.10	17.19	0.290	...	− 4.704
54	EK Dra	G5V	07.61	0.640	02.67	34.12	− 0.631	− 3.553	− 3.887
55	HD 142373	F9V	04.62	0.560	15.00	15.89	0.353	...	− 5.210
56	MS Ser	K2V	08.21	1.000	09.59	77.14	− 0.380	− 3.564	− 3.760
57	HD 154417	F9V	06.01	0.580	07.80	20.66	0.004	− 4.946	− 4.359
58	HD 182101	F6V	06.36	0.400	02.00	37.55	0.223	− 5.139	− 4.496
59	HD 187013	F7V	04.99	0.470	06.40	21.23	0.347	− 5.471	− 4.639
60	HD 201091	K5V	05.21	1.180	37.90	03.48	0.200	− 5.256	− 4.448
61	HD 206860	G0V	05.95	0.580	04.70	17.88	− 0.230	− 4.462	− 4.194

Notes. D is distance.

⋆Parameters derived in this paper.

Table 2. Degree of polarization and polarization angle of late-type active dwarfs in *B*, *V*, *R*, and *I* bands.

Object	Mean epoch*	*B*-Filter		*V*-Filter		*R*-Filter		*I*-Filter	
	(HJD)	*P* (per cent)	$\theta(^\circ)$	*P* (per cent)	$\theta(^\circ)$	*P* (per cent)	$\theta(^\circ)$	*P* (per cent)	$\theta(^\circ)$
PW And	2456948.1136	0.216 ± 0.043	40 ± 5	0.099 ± 0.041	93 ± 6	0.059 ± 0.085	157 ± 15	0.034 ± 0.013	25 ± 3
	2456949.0839	0.211 ± 0.032	86 ± 5	0.079 ± 0.019	75 ± 3	0.098 ± 0.072	91 ± 11	0.053 ± 0.086	103 ± 16
BK Psc	2455854.2780	0.250 ± 0.076	81 ± 6	0.082 ± 0.043	77 ± 7	0.065 ± 0.027	122 ± 6	0.033 ± 0.011	101 ± 3
BD−04234	2456982.1425	0.473 ± 0.099	46 ± 5	0.095 ± 0.053	136 ± 8	0.079 ± 0.072	98 ± 35	0.039 ± 0.024	174 ± 5
	2456982.5918	0.359 ± 0.027	33 ± 3	0.093 ± 0.080	113 ± 21	0.054 ± 0.038	132 ± 8	0.047 ± 0.034	71 ± 7
V1221 Tau	2455887.2871	0.151 ± 0.029	9 ± 3	0.066 ± 0.058	80 ± 17	0.040 ± 0.064	33 ± 13	0.028 ± 0.051	82 ± 20
V988 Tau	2455886.3006	0.143 ± 0.018	11 ± 2	0.072 ± 0.043	47 ± 17	0.044 ± 0.028	49 ± 6	0.042 ± 0.076	161 ± 15
	2456003.1265	0.142 ± 0.074	15 ± 15	0.064 ± 0.034	149 ± 6	0.050 ± 0.070	130 ± 13	0.048 ± 0.076	19 ± 15
V526 Aur	2455559.3357	0.413 ± 0.068	155 ± 4	0.474 ± 0.042	179 ± 3	0.405 ± 0.091	170 ± 5	0.362 ± 0.027	176 ± 2
	2455601.1475	0.678 ± 0.021	168 ± 2	0.669 ± 0.044	177 ± 2	0.606 ± 0.035	178 ± 1	0.610 ± 0.025	175 ± 1
V538 Aur	2456978.7681	0.302 ± 0.026	28 ± 3	0.090 ± 0.042	86 ± 13	0.058 ± 0.078	22 ± 15	0.044 ± 0.010	133 ± 3
V848 Mon	2455886.3394	0.151 ± 0.010	20 ± 2	0.065 ± 0.023	91 ± 10	0.061 ± 0.026	158 ± 55	0.037 ± 0.070	122 ± 15
	2456002.1748	0.162 ± 0.012	64 ± 2	0.098 ± 0.141	75 ± 20	0.052 ± 0.048	19 ± 9	0.050 ± 0.030	129 ± 4
V850 Mon	2455887.3991	0.197 ± 0.040	11 ± 4	0.086 ± 0.045	98 ± 15	0.050 ± 0.010	46 ± 3	0.032 ± 0.013	110 ± 3
	2456036.0566	0.208 ± 0.030	173 ± 4	0.085 ± 0.057	143 ± 9	0.062 ± 0.034	82 ± 6	0.038 ± 0.031	17 ± 7
V429 Gem	2456978.8045	0.268 ± 0.028	60 ± 9	0.113 ± 0.077	12 ± 20	0.083 ± 0.062	173 ± 10	0.070 ± 0.035	173 ± 10
	2456980.3207	0.261 ± 0.058	24 ± 6	0.106 ± 0.053	179 ± 7	0.087 ± 0.034	61 ± 13	0.064 ± 0.021	180 ± 3
V867 Mon	2455886.3711	0.117 ± 0.088	169 ± 12	0.051 ± 0.039	145 ± 7	0.032 ± 0.081	141 ± 18	0.056 ± 0.070	122 ± 13
	2456015.1162	0.160 ± 0.026	4 ± 3	0.064 ± 0.026	35 ± 5	0.042 ± 0.010	132 ± 2	0.045 ± 0.052	100 ± 10
BD+231799	2455603.2027	0.165 ± 0.020	147 ± 2	0.065 ± 0.021	14 ± 4	0.044 ± 0.068	158 ± 13	0.042 ± 0.076	41 ± 15
	2456002.2215	0.141 ± 0.010	56 ± 2	0.078 ± 0.059	24 ± 10	0.041 ± 0.057	139 ± 13	0.034 ± 0.010	97 ± 2
HO Cnc	2455886.4332	0.264 ± 0.020	33 ± 2	0.102 ± 0.028	19 ± 4	0.071 ± 0.035	22 ± 14	0.045 ± 0.027	56 ± 5
	2455972.2458	0.221 ± 0.014	165 ± 3	0.103 ± 0.064	27 ± 18	0.058 ± 0.022	140 ± 10	0.044 ± 0.039	92 ± 26
HP Cnc	2455887.4411	0.135 ± 0.016	36 ± 2	0.057 ± 0.021	38 ± 4	0.038 ± 0.014	47 ± 3	0.030 ± 0.054	86 ± 12
	2455972.2841	0.152 ± 0.074	79 ± 14	0.084 ± 0.059	98 ± 9	0.064 ± 0.024	149 ± 11	0.034 ± 0.076	90 ± 16
V402 Hya	2456036.0990	0.265 ± 0.093	16 ± 7	0.090 ± 0.052	57 ± 17	0.068 ± 0.052	11 ± 22	0.044 ± 0.062	91 ± 12
V405 Hya	2455559.4573	0.114 ± 0.017	113 ± 2	0.067 ± 0.010	92 ± 3	0.025 ± 0.042	104 ± 48	0.044 ± 0.037	127 ± 7
	2455602.3067	0.151 ± 0.067	114 ± 8	0.056 ± 0.021	94 ± 4	0.048 ± 0.023	98 ± 5	0.039 ± 0.046	53 ± 10
GT Leo	2455588.3479	0.117 ± 0.011	174 ± 3	0.056 ± 0.066	85 ± 34	0.037 ± 0.041	95 ± 10	0.025 ± 0.031	101 ± 5
	2455593.3627	0.130 ± 0.082	103 ± 10	0.071 ± 0.045	146 ± 8	0.032 ± 0.037	80 ± 7	0.044 ± 0.005	2 ± 2
V417 Hya	2455956.3962	0.131 ± 0.014	39 ± 3	0.069 ± 0.059	22 ± 10	0.038 ± 0.069	133 ± 14	0.031 ± 0.016	39 ± 3
	2455986.3307	0.124 ± 0.053	178 ± 12	0.074 ± 0.018	75 ± 7	0.055 ± 0.037	101 ± 19	0.038 ± 0.030	124 ± 6
LR Hya	2456984.0450	0.181 ± 0.033	94 ± 5	0.125 ± 0.011	100 ± 2	0.081 ± 0.037	84 ± 6	0.032 ± 0.015	84 ± 13
	2456984.5619	0.135 ± 0.028	19 ± 15	0.089 ± 0.023	17 ± 4	0.060 ± 0.003	75 ± 3	0.042 ± 0.024	135 ± 5
V418 Hya	2456002.2661	0.120 ± 0.016	26 ± 2	0.059 ± 0.032	69 ± 6	0.038 ± 0.010	174 ± 2	0.022 ± 0.045	60 ± 11
	2456035.0968	0.112 ± 0.048	97 ± 7	0.064 ± 0.021	110 ± 14	0.074 ± 0.045	109 ± 9	0.035 ± 0.030	94 ± 7
AB Crt	2456001.2376	0.211 ± 0.010	24 ± 2	0.092 ± 0.010	32 ± 2	0.056 ± 0.019	71 ± 10	0.042 ± 0.011	21 ± 2
	2456015.2655	0.247 ± 0.032	85 ± 4	0.088 ± 0.030	22 ± 5	0.057 ± 0.010	176 ± 2	0.040 ± 0.024	61 ± 5
HL Leo	2455578.7580	0.082 ± 0.066	49 ± 10	0.035 ± 0.020	60 ± 16	0.035 ± 0.036	163 ± 30	0.024 ± 0.030	57 ± 10
	2455603.3665	0.095 ± 0.020	70 ± 6	0.032 ± 0.070	153 ± 15	0.030 ± 0.100	18 ± 22	0.026 ± 0.052	67 ± 11
GQ Leo	2456036.1684	0.248 ± 0.049	81 ± 4	0.092 ± 0.059	72 ± 3	0.065 ± 0.031	62 ± 5	0.044 ± 0.037	78 ± 7
	2456092.1181	0.222 ± 0.026	57 ± 3	0.078 ± 0.040	77 ± 10	0.086 ± 0.010	117 ± 2	0.042 ± 0.031	38 ± 8
PQ Vir	2455603.4791	0.144 ± 0.027	69 ± 3	0.071 ± 0.020	108 ± 8	0.059 ± 0.010	88 ± 2	0.025 ± 0.064	99 ± 15
	2455955.3870	0.137 ± 0.072	46 ± 9	0.055 ± 0.011	42 ± 2	0.048 ± 0.023	140 ± 14	0.029 ± 0.016	58 ± 4
MY UMa	2456001.2803	0.140 ± 0.011	31 ± 2	0.061 ± 0.034	139 ± 6	0.056 ± 0.015	95 ± 3	0.033 ± 0.040	116 ± 9
	2456013.3025	0.151 ± 0.086	87 ± 16	0.078 ± 0.044	115 ± 7	0.057 ± 0.012	68 ± 6	0.034 ± 0.010	154 ± 2
PR Vir	2455955.4279	0.214 ± 0.081	99 ± 11	0.081 ± 0.016	44 ± 6	0.055 ± 0.033	150 ± 6	0.064 ± 0.025	104 ± 11
	2455986.3740	0.209 ± 0.016	109 ± 2	0.076 ± 0.048	14 ± 8	0.058 ± 0.012	136 ± 3	0.061 ± 0.050	118 ± 9
FZ Leo	2456019.3231	0.112 ± 0.024	25 ± 3	0.054 ± 0.016	56 ± 3	0.039 ± 0.029	120 ± 10	0.029 ± 0.059	42 ± 9
	2456035.1380	0.103 ± 0.092	41 ± 13	0.053 ± 0.036	67 ± 7	0.036 ± 0.025	106 ± 20	0.024 ± 0.031	123 ± 7
LV Com	2455588.4741	0.150 ± 0.028	110 ± 6	0.087 ± 0.023	91 ± 4	0.061 ± 0.047	2 ± 22	0.066 ± 0.069	122 ± 12
	2455602.4095	0.126 ± 0.052	37 ± 12	0.053 ± 0.017	77 ± 3	0.047 ± 0.056	160 ± 11	0.058 ± 0.057	144 ± 8
DO CVn	2456001.3195	0.133 ± 0.060	40 ± 8	0.068 ± 0.056	51 ± 9	0.047 ± 0.052	105 ± 10	0.029 ± 0.010	114 ± 2
	2456004.3271	0.151 ± 0.020	34 ± 4	0.060 ± 0.018	34 ± 8	0.050 ± 0.015	149 ± 9	0.025 ± 0.025	99 ± 6
LX Com	2455602.4754	0.157 ± 0.061	124 ± 7	0.087 ± 0.013	143 ± 2	0.044 ± 0.068	105 ± 14	0.021 ± 0.042	134 ± 12
	2455956.4363	0.137 ± 0.014	44 ± 2	0.070 ± 0.022	166 ± 9	0.061 ± 0.018	10 ± 3	0.026 ± 0.038	165 ± 43
PX Vir	2456984.5779	0.213 ± 0.091	62 ± 8	0.135 ± 0.035	60 ± 4	0.076 ± 0.055	48 ± 21	0.065 ± 0.020	33 ± 4
GY Boo	2456002.4543	0.120 ± 0.010	44 ± 2	0.045 ± 0.022	112 ± 14	0.031 ± 0.002	102 ± 2	0.026 ± 0.032	135 ± 7
	2456015.4263	0.124 ± 0.019	42 ± 4	0.049 ± 0.050	98 ± 10	0.050 ± 0.060	138 ± 12	0.047 ± 0.042	110 ± 8
GZ Boo	2456016.4076	0.207 ± 0.010	82 ± 2	0.080 ± 0.042	46 ± 16	0.066 ± 0.012	6 ± 2	0.033 ± 0.075	148 ± 65
	2456036.3709	0.204 ± 0.073	60 ± 7	0.086 ± 0.038	42 ± 6	0.059 ± 0.021	92 ± 4	0.038 ± 0.088	128 ± 18

Table 2 – *continued*

Object	Mean epoch⋆ (HJD)	*B*-Filter		*V*-Filter		*R*-Filter		*I*-Filter	
		P (per cent)	$\theta(^\circ)$	*P* (per cent)	$\theta(^\circ)$	*P* (per cent)	$\theta(^\circ)$	*P* (per cent)	$\theta(^\circ)$
HO Boo	2455986.4308	0.134 ± 0.095	148 ± 20	0.055 ± 0.014	144 ± 3	0.036 ± 0.057	71 ± 12	0.021 ± 0.018	115 ± 4
	2456002.4285	0.117 ± 0.051	49 ± 7	0.049 ± 0.048	43 ± 9	0.036 ± 0.013	106 ± 3	0.020 ± 0.080	143 ± 20
FN Boo	2455294.2500	0.250 ± 0.024	95 ± 6	0.087 ± 0.011	103 ± 3	0.054 ± 0.011	99 ± 2	0.021 ± 0.037	85 ± 10
	2455337.3210	0.234 ± 0.010	132 ± 2	0.082 ± 0.020	127 ± 2	0.027 ± 0.098	147 ± 23	0.032 ± 0.087	64 ± 20
V1022 Her	2456091.2666	0.302 ± 0.086	49 ± 6	0.122 ± 0.025	16 ± 3	0.080 ± 0.015	173 ± 5	0.057 ± 0.049	119 ± 25
	2456094.1142	0.300 ± 0.071	54 ± 5	0.142 ± 0.052	67 ± 6	0.078 ± 0.034	110 ± 14	0.050 ± 0.051	100 ± 9
V1658 Aql	2455854.0749	0.443 ± 0.052	75 ± 4	0.418 ± 0.058	82 ± 3	0.350 ± 0.081	89 ± 5	0.370 ± 0.021	88 ± 2
	2455886.0550	0.659 ± 0.101	98 ± 4	0.762 ± 0.118	99 ± 4	0.639 ± 0.146	84 ± 7	0.627 ± 0.131	81 ± 13
V1659 Aql	2455854.0749	0.550 ± 0.047	82 ± 2	0.575 ± 0.041	76 ± 2	0.535 ± 0.023	96 ± 2	0.530 ± 0.080	88 ± 4
	2455886.0550	0.555 ± 0.012	78 ± 1	0.550 ± 0.032	89 ± 2	0.550 ± 0.064	103 ± 3	0.498 ± 0.054	91 ± 3
V401 Vul	2455890.0710	0.234 ± 0.054	9 ± 5	0.129 ± 0.106	75 ± 13	0.065 ± 0.048	4 ± 21	0.030 ± 0.011	121 ± 3
V402 Peg	2456948.0589	0.102 ± 0.036	26 ± 5	0.040 ± 0.078	82 ± 16	0.030 ± 0.065	122 ± 8	0.022 ± 0.039	18 ± 33
	2456949.0326	0.115 ± 0.024	68 ± 10	0.030 ± 0.064	163 ± 14	0.024 ± 0.053	103 ± 35	0.014 ± 0.045	164 ± 24
OT Peg	2455527.1293	0.161 ± 0.039	78 ± 4	0.055 ± 0.025	80 ± 4	0.054 ± 0.010	67 ± 2	0.031 ± 0.004	37 ± 2
	2455559.0736	0.152 ± 0.076	96 ± 7	0.078 ± 0.010	121 ± 2	0.039 ± 0.054	111 ± 11	0.026 ± 0.031	103 ± 8
V383 Lac	2456949.0679	0.116 ± 0.059	33 ± 8	0.066 ± 0.027	176 ± 5	0.033 ± 0.012	28 ± 3	0.015 ± 0.042	85 ± 10
	2456948.0992	0.128 ± 0.039	168 ± 9	0.088 ± 0.058	105 ± 9	0.060 ± 0.017	70 ± 13	0.028 ± 0.065	80 ± 10
HD 218782	2455886.1614	0.265 ± 0.042	27 ± 3	0.166 ± 0.015	49 ± 2	0.078 ± 0.080	101 ± 13	0.045 ± 0.078	78 ± 15

Note. ⋆Mean epoch of *B*, *V*, *R* and *I* observations.

agreement with the average value of R_V (=3.1) for the Milky Way Galaxy, indicating that the sizes of the dust grains in the direction of these stars are normal.

3.2 Polarization due to magnetic intensification (MI)

Polarization due to MI has been modelled in a number of studies, and the degree of polarization has been assumed to depend linearly on the size of magnetized region of cool stars (e.g. Mullan & Bell 1976; Calamai & Degl'Innocenti 1983; Degl'Innocenti 1983; Huovelin & Saar 1991). Later Saar & Huovelin (1993) demonstrated that this dependence is non-linear for large magnetic regions, and they developed a model for the wavelength dependence of BLP. The magnetic area relative to the observer must be asymmetrically distributed for net polarization to result. Thus polarization can range from zero up to a maximum value $P_{\rm MI}$ for a given filling factor, depending on the exact arrangement of magnetic regions on the surface. In particular, for a single circular region, the degree of polarization will be proportional to a factor of *A*, which approximately depends on the area of the magnetic region (*f* in per cent). The maximum expected polarization due to MI is given by Saar & Huovelin (1993) as

$$P_{\rm MI} \approx \frac{4}{3\pi}\frac{\xi}{1-\xi}A(f)\Pi\left(\theta=\frac{\pi}{2}\right), \quad (3)$$

where $A(f) \approx -2.128 \times 10^{-4} + 1.076f - 4.812f^2 + 9.058f^3 - 6.26f^4$, θ is angle between the magnetic field and the line of sight, ξ is fractional line blanketing and Π is polarized amplitude. Saar & Huovelin (1993) have calculated a grid of expected degrees of polarization in *U*, *B*, *V*, *R* and *I* bands for the stars with temperature ranging from 4000 to 7000 K, log g from 2.0 to 4.5 and for maximum spot area of 24 per cent. We have used their results to compare with our observed values of average polarization of active dwarfs. The degree of polarization in *B*, *V*, *R* and *I* bands with their theoretical values are shown in Fig. 4, where the theoretical values are represented by continuous thick lines. The observed values of polarization for 12 stars (HP Cnc, FZ Leo, OT Peg, HL Leo, HO Boo, GT Leo, V418 Hya, V401 Vul, BK Psc, V402 Peg, V867 Mon and V988 Tau) are found to be well within 1σ level to the theoretical values of the polarization due to MI. However, there are 22 stars where MI polarizations are within 1–3σ from the observed one. The observed values of polarization in six stars (V1221 Tau, HD 218782, V848 Mon, BD+23° 1799 and V538 Aur) in the sample are found to be above the 3σ level from the MI polarizations.

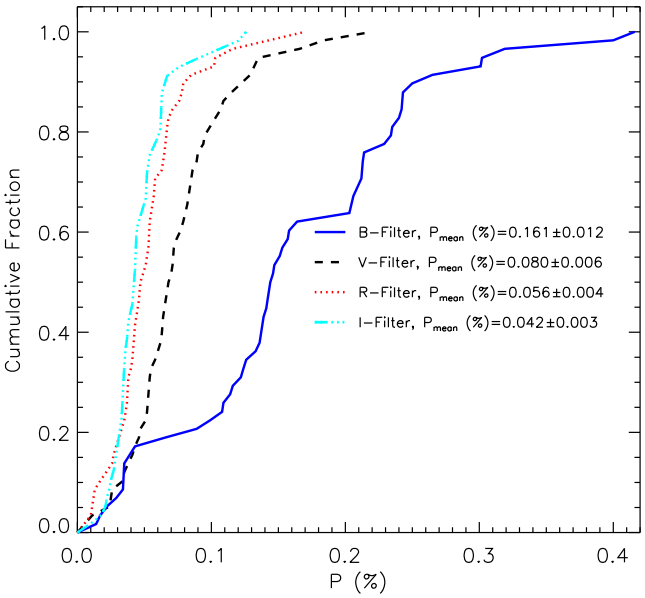

Figure 1. Cumulative distribution of degree of polarization in *B*, *V*, *R*, and *I* bands.

3.3 Polarization due to scattering

There are 28 stars, where the observed polarization are well above the 1σ level from the MI polarization, indicating that polarization in these stars may be due to additional sources like scattering. The

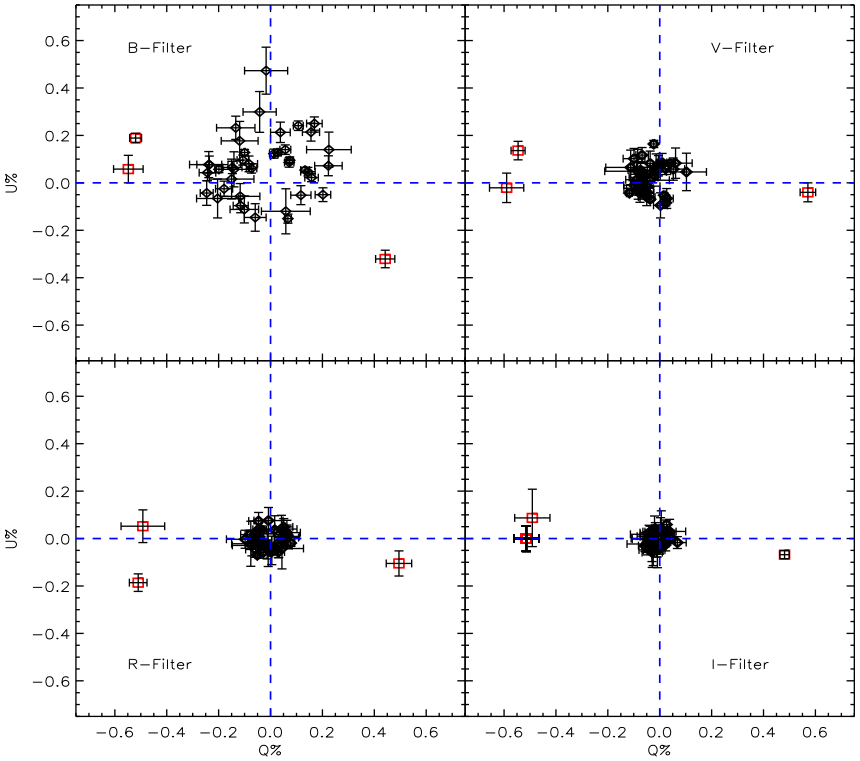

Figure 2. Q versus U diagram for the active dwarfs in *B*, *V*, *R*, and *I* bands.

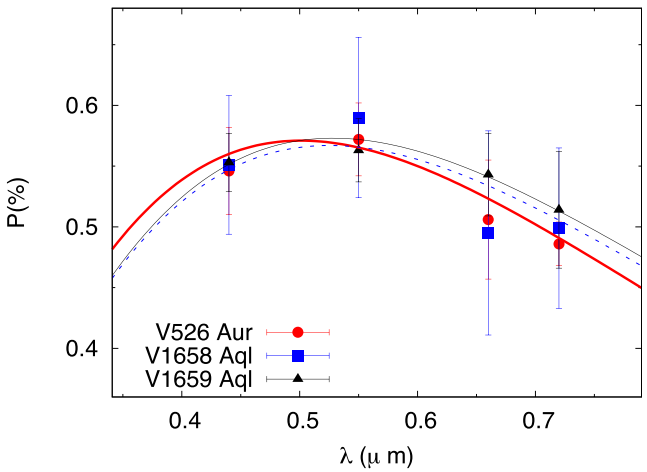

Figure 3. The best-fitting Serkowski law for the stars V526 Aur, V1658 Aql and V1659 Aql.

extended inhomogeneous envelopes, chromospheres and photospheric spots could be a possible source of scattering induced BLP in late-type stars. Stars with chromospheres may also have enough free electrons to cause linear polarization via Thomson scattering (TS), similar to the envelopes of early type stars (Serkowski 1970; Brown & McLean 1977). However, it has been shown that TS is negligible and Rayleigh scattering is probably a significant contributor to the total BLP. Saar & Huovelin (1993) derived models which are suitable for the atmospheres of cool stars and to distinguish between scattering and MI as a sources of BLP. These models employed an optimum value for the scattering optical depth (τ_s) of 0.1, whereas for the solar type stars, τ_s is generally less than 0.1. A difference in τ_s or in the incident intensity between an asymmetrically distributed region and the surrounding stellar atmosphere is necessary to produce net BLP due to scattering in a star. A horizontally uniform atmospheric layer with uniform incident intensity will yield zero disc-integrated BLP for a layer of any τ_s. Net scattering induced BLP can be produced by an anisotropic incident light, occurring near the star-spots (Finn & Jefferies 1974). Saar & Huovelin (1993) derived the following relation for scattering induced BLP

$$P_{\rm scat} = \frac{3\epsilon}{16(3-\epsilon)}\tau_s A_s(f), \quad (4)$$

where $A_s(f) \approx 1.192 \times 10^{-4} + 1.048f - 6.945f^2 + 22.46f^3 - 35.92f^4 + 22.55f^5$ and ϵ is the limb darkening coefficient. The maximum scattering polarization for a maximum spot coverage of 18 per cent are computed in *B*, *V*, *R*, and *I* bands by using the linear limb darkening coefficients from Claret & Bloemen (2011) and $\tau_s = 0.1$. We have used these maximum scattering polarization values to compare with observed polarization values. The maximum scattering polarization for these dwarfs in the sample are shown in Fig. 4 with open circles. One can see that maximum polarizations due to the scattering are much smaller in comparison to the observed polarizations and also less than the polarizations due to MI. This indicates that scattering alone is not responsible for net BLP in these active dwarfs.

3.4 Polarization due to MI plus scattering

As we have discussed above, the BLP calculated theoretically as arising either due to MI or due to scattering has been found to be less than the observed polarization of majority of stars in the sample. Therefore, in order to see the combined effect of MI and scattering, we have added theoretical maximum values of polarization due to

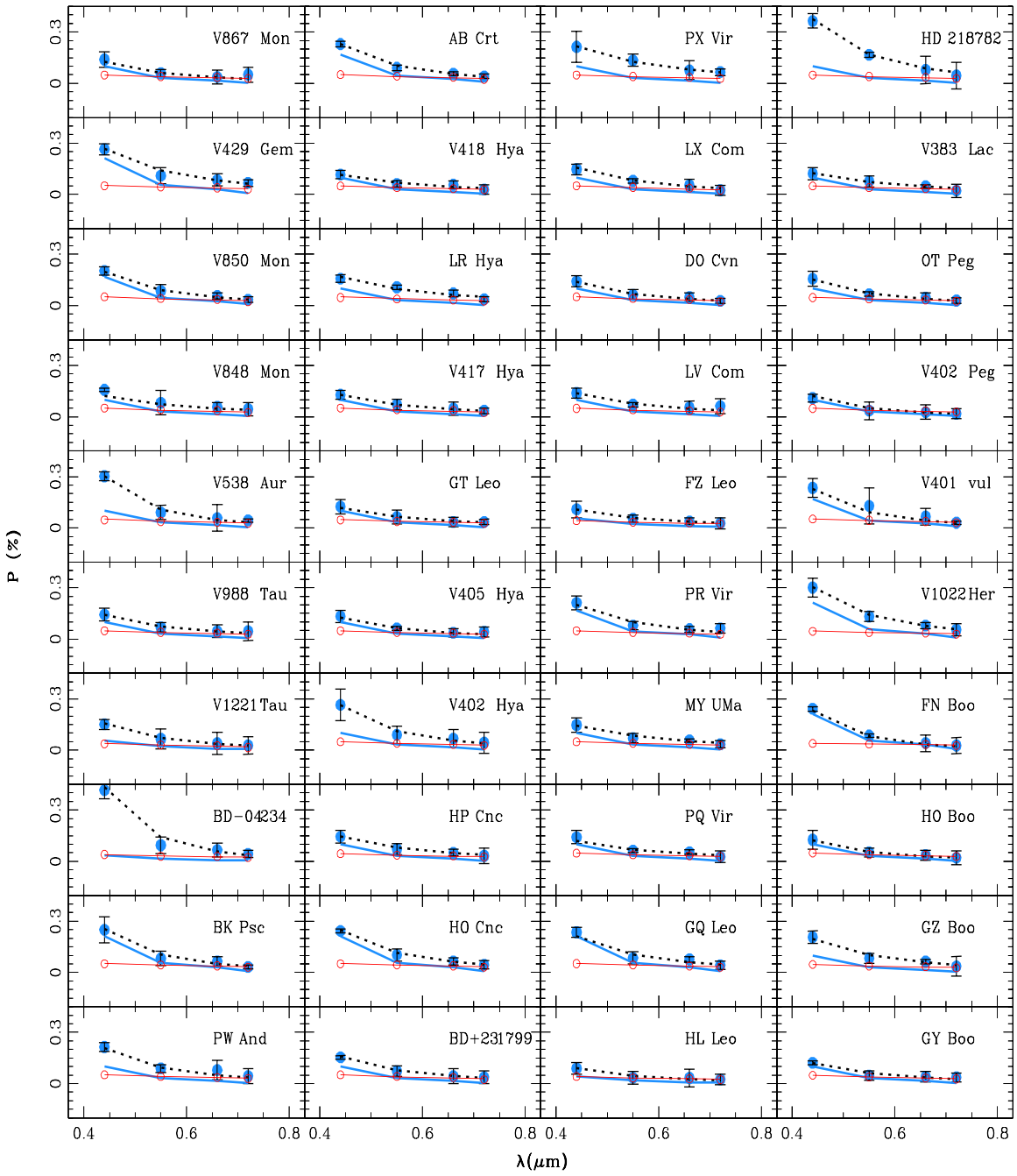

Figure 4. Degree of polarization as a function of wavelength for active dwarfs in the sample. The thick continuous lines show the theoretical values of the degree of polarization expected for a Zeeman polarization model. The solid circles with dotted line show the observed values of the degree of polarization. The open circles with continuous line show maximum value of polarization due to scattering.

MI and due to scattering. The resultant values are compared with observed polarization values for all the stars in the sample. The observed polarization in 29 stars in our sample are found to be well within 1σ level to that from the polarizations due to MI plus scattering. However, there are nine stars (PW And, PX Vir, V402 Peg, V1221 Tau, V402 Hya, HD 218782, GZ Boo, GY Boo and HO Cnc), where combined values of polarization due to the MI and scattering are found to be within 1–3σ of the observed values. The observed polarizations in two stars (BD-04° 234 and V538 Aur) are found to be more than the 3σ level of the polarization due to MI plus scattering, indicating supplementary sources of polarization.

4 LINEAR POLARIZATION AS A FUNCTION OF DIFFERENT ACTIVITY PARAMETERS

4.1 The $(B - V)$ colour

The behaviour of degree of linear polarization P and $(B - V)$ colour in B, V, R, and I bands is displayed in Fig. 5. The degree of polarization is found to be increasing towards later spectral type from $(B - V) = 0.400$ to 1.504. Results of various correlations are given in Table 3. The correlation coefficients between BLP and $(B - V)$ colour are found to be 0.55, 0.41, 0.37, and 0.15 in B, V, R, and I bands, respectively. The probability of correlation is found to be

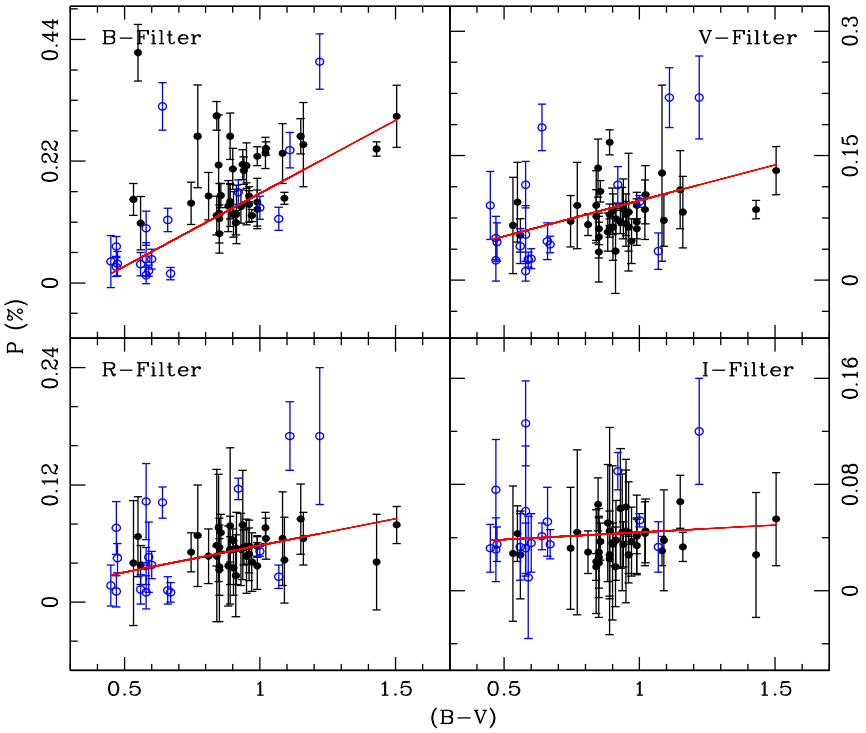

Figure 5. Dependence of degree of polarization P on the colour index $(B - V)$ in B, V, R, and I bands where solid and open circles represent present data and literature data, respectively, and continuous straight line are the linear regression fit.

Table 3. Parameters as obtained from the linear regression fit between degree of polarization and various activity parameters along with the correlation coefficient (r) and probability of no correlation (q), where m and c are slope and intercept.

Filter	m	c	r	q
Colour($B-V$)				
B	0.26 ± 0.03	−0.09 ± 0.03	0.55	8.844×10^{-6}
V	0.09 ± 0.02	−0.003 ± 0.016	0.41	0.001
R	0.05 ± 0.01	0.004 ± 0.014	0.37	0.004
I	0.014 ± 0.009	0.029 ± 0.010	0.15	0.264
Rosby number(R_0)				
B	−0.12 ± 0.02	0.08 ± 0.01	−0.689	8.517×10^{-9}
V	−0.051 ± 0.009	0.049 ± 0.006	−0.625	4.328×10^{-7}
R	−0.042 ± 0.007	0.035 ± 0.004	−0.534	3.231×10^{-5}
I	−0.010 ± 0.006	0.038 ± 0.004	−0.275	0.044
(R′HK)				
B	0.094 ± 0.044	0.517 ± 0.189	0.479	0.001
V	0.062 ± 0.014	0.325 ± 0.061	0.459	0.002
R	0.033 ± 0.010	0.186 ± 0.041	0.492	0.001
I	0.024 ± 0.007	0.142 ± 0.028	0.357	0.017
($R_X = L_X/L_{bol}$)				
B	0.059 ± 0.012	0.358 ± 0.051	0.644	1.369×10^{-6}
V	0.029 ± 0.007	0.195 ± 0.029	0.508	0.0003
R	0.020 ± 0.005	0.132 ± 0.020	0.423	0.0034
I	0.008 ± 0.004	0.074 ± 0.014	0.149	0.3229

more than 99 per cent in B, V, and R bands. However, the correlation in I band is found to be only 70 per cent (see Table 3). The slopes between P and $(B - V)$ are found to be 0.26 ± 0.03, 0.09 ± 0.02, 0.05 ± 0.01 and 0.014 ± 0.009 in the B, V, R and I bands, respectively.

4.2 Rossby number

The Rossby number (R_o) is defined as the ratio of rotational period (P_{rot}) and the convective turn over time (τ_c). The following empirical relation for the convective turn over time in terms of $(B - V)$ has been derived by Noyes et al. (1984) by assuming an intermediate value of ratio of mixing length to scaleheight (=1.9).

$$\log \tau_c = \begin{pmatrix} 1.362 - 0.166x + 0.025x^2 - 5.323x^3, x > 0 \\ 1.362 - 0.14x, x < 0 \end{pmatrix}, \quad (5)$$

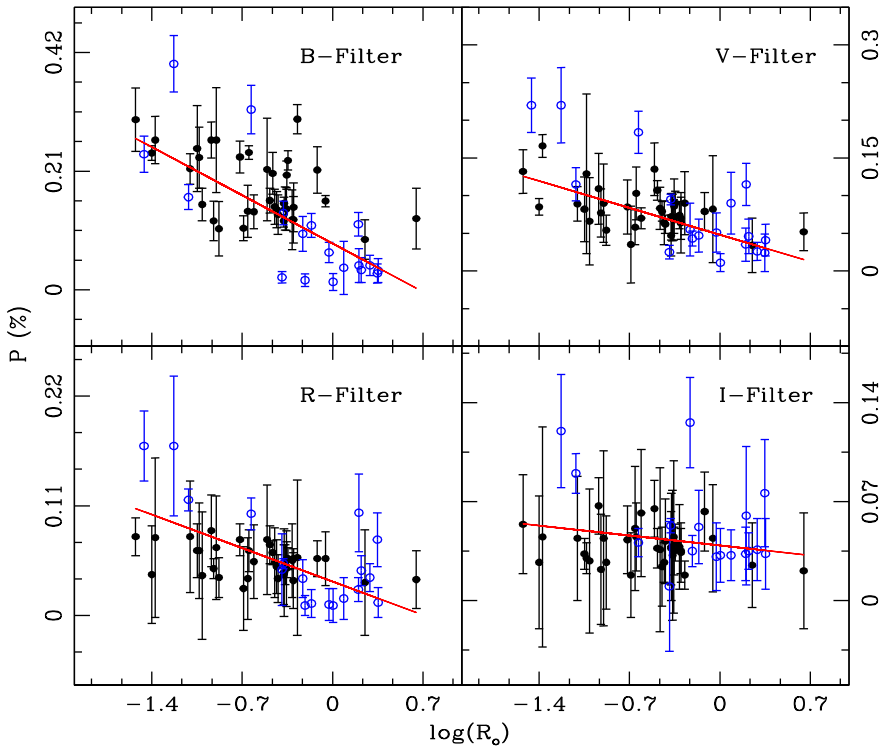

Figure 6. Degree of polarization P versus Rossby number R_0 in B, V, R, and I bands, where symbols are similar to Fig. 5. Straight lines are linear regression fit.

where $x = 1 - (B - V)$. Making use of this relation we computed values of R_o and the results are given in Table 1. The plots between P and R_0 in the B, V, R, and I bands are shown in Fig. 6. It is easy to infer from the table that the polarization in B band is strongly dependent on the R_O i.e. the polarization increases with decreasing Rossby number. The dependence of polarization on the R_O is weak towards longer wavelength. Correlation coefficients for P and log R_O correlation in B, V, R, and I bands have been determined to be of −0.69, −0.63, −0.53, and −0.28, respectively. The statistical significance of the correlations are found to be more than 99 per cent in each of B, V, and R bands but for I band no significant correlation was found (see Table 3). The slopes of linear regression fit between these two quantities in the B, V, R, and I are found to be −0.12 ± 0.02, −0.051 ± 0.009, −0.042 ± 0.007, and −0.010 ± 0.006, respectively.

4.3 Chromospheric activity index

The chromospheric activity index ($R'_{\rm HK}$) is measured from chromospheric emission in the cores of the broad photospheric Ca II H & K absorption lines, normalized to the underlying photospheric spectrum. $R'_{\rm HK}$ is calculated from a band ratio measurement of the Ca II H & K emission line strength S-index (Vaughan, Preston & Wilson 1978; Vaughan & Preston 1980; Duncan et al. 1991) and is given as

$$R'_{\rm HK} = \frac{F'_{\rm HK}}{\sigma T_{\rm eff}^4} \tag{6}$$

where σ is Stefan–Boltzman constant and $F'_{\rm HK} = 1.6 \times 10^6 (10^{-14} S C_{\rm ef} T_{\rm eff}^4) - F_{0,\rm HK}$ is an excess flux. The conversion factor ($C_{\rm ef}$), basal flux ($F_{0,\rm HK}$), and effective temperature ($T_{\rm eff}$) are functions of $(B - V)$, and for main-sequence stars, the empirical relations for these quantities are given as (Middelkoop 1982; Rutten 1984)

$$\log(C_{\rm ef}) = 0.25(B-V)^3 - 1.33(B-V)^2 + 0.43(B-V) + 0.24. \tag{7}$$

$$\log(F_{0,\rm HK}) = 1.83 - 2.76(B-V), \quad \text{for } 0.3 < (\rm B-V) < 0.48$$
$$= 7.79 - 2.23(B-V), \quad \text{for } 0.48 < (\rm B-V) < 1.25. \tag{8}$$

$$\log(T_{\rm eff}) = 4.04 - 0.71(B-V) + 0.55(B-V)^2 - 0.20(B-V)^3. \tag{9}$$

In order to calculate the values $R'_{\rm HK}$, we have taken the mean of highest and lowest values S-index from Pace (2013). The resulting logarithmic values of $R'_{\rm HK}$ are given in Table 1. The dependence of the degree of polarization on $R'_{\rm HK}$ in B, V, R, and I bands are shown in Fig 7, and results of correlations are given in Table 3. The solid lines in the figure show the best-fitting straight lines with the slopes as 0.094 ± 0.044, 0.062 ± 0.014, 0.033 ± 0.010, and 0.024 ± 0.007 in the B, V, R, and I, respectively. It is observed that the value of slopes have its highest values in the B band and the smallest in the I band. Positive correlations between P and $\log(R'_{\rm HK})$ are found with correlation coefficients of 0.479, 0.459, 0.492, and 0.357 in B, V, R, and I bands, respectively. These correlations are found above 98.3 per cent confidence level.

4.4 Coronal activity index

The coronal activity index ($R_{\rm X}$) is defined as the ratio of X-ray luminosity ($L_{\rm X}$) to the bolometric luminosity ($L_{\rm bol}$). The $L_{\rm X}$ of

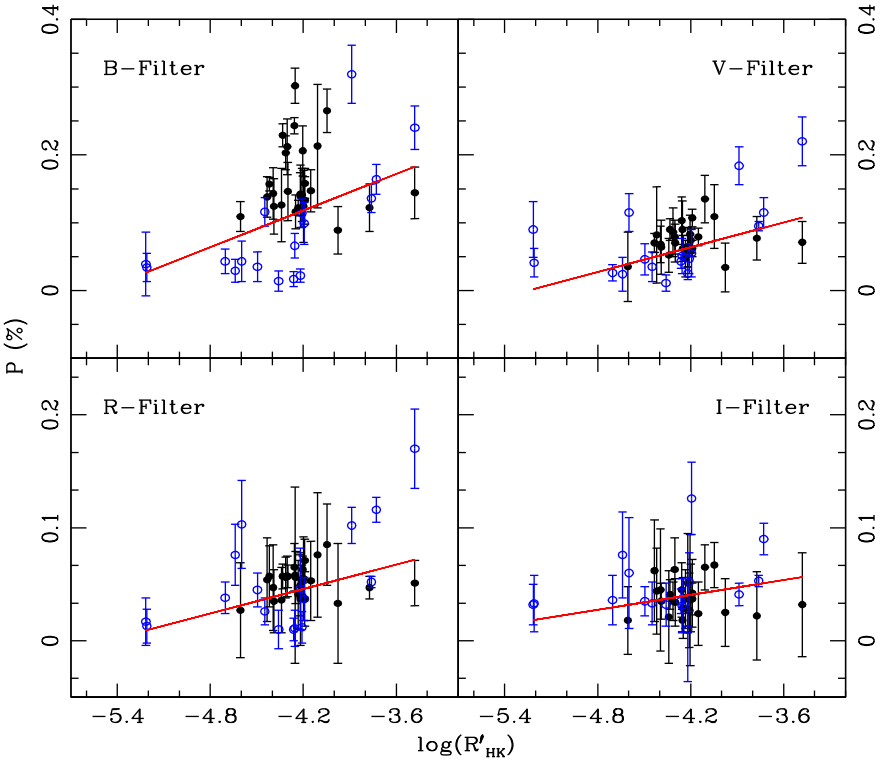

Figure 7. Degree of polarization P versus $\log(R'_{\rm HK})$ in B, V, R, and I bands, where symbols are similar to Fig. 5. Straight lines are the linear regression fit.

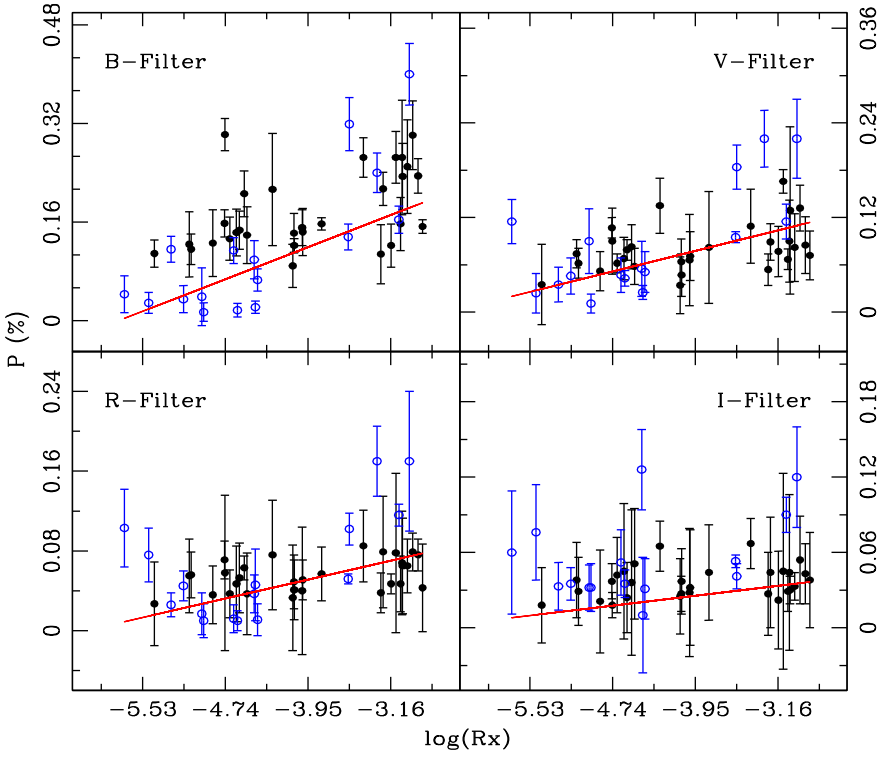

Figure 8. Degree of polarization P versus $\log(R_{\rm X})$ in B, V, R, and I bands, where symbols are similar to Fig 5. Straight lines are the linear regression fit.

the active dwarfs in the sample are calculated by using relation $L_{\rm X} = 4\pi D^2 C_{\rm X} f_{\rm X}$, where D is the distance of the star in cm, $f_{\rm X}$ is the count rate in counts s^{-1} in the 0.1–2.4 keV energy band, and $C_{\rm X} = (8.31 + 5.30HR) \times 10^{-12}$ erg cm^{-2} $counts^{-1}$, is a conversion factor. The count rate and hardness ratio (HR) were taken from *ROSAT* All Sky Survey (Voges et al. 1999). The derived values of $R_{\rm X}$ are given in Table 1. Fig. 8 shows the correlation between degree of polarization and $R_{\rm X}$ in B, V, R, and I bands, where solid lines are the

Table 4. Values of 'b' in the relation $P \propto \lambda^{-b}$ for the polarization due to MI and scattering, and observed polarization.

S.No	Object	b_M	b_S	b_{MS}	b_O
1	PW And	5.1 ± 0.4	1.0 ± 0.1	2.9 ± 0.2	3.6 ± 0.5
2	BK Psc	5.6 ± 0.5	0.9 ± 0.2	3.8 ± 0.4	3.9 ± 0.5
3	BD−04234	4.0 ± 0.2	1.0 ± 0.2	2.1 ± 0.1	5.0 ± 0.7
4	V1221 Tau	4.3 ± 0.2	1.3 ± 0.4	2.7 ± 0.2	3.5 ± 0.1
5	V988 Tau	5.1 ± 0.4	1.0 ± 0.1	3.0 ± 0.2	2.9 ± 0.3
6	V538 Aur	5.1 ± 0.4	1.1 ± 0.1	3.0 ± 0.2	4.6 ± 0.5
7	V848 Mon	5.1 ± 0.4	1.2 ± 0.3	3.0 ± 0.3	2.6 ± 0.1
8	V850 Mon	5.5 ± 0.6	1.2 ± 0.3	3.6 ± 0.4	3.4 ± 0.2
9	V429 Gem	5.6 ± 0.5	0.9 ± 0.2	3.8 ± 0.4	2.9 ± 0.3
10	V867 Mon	5.1 ± 0.4	1.0 ± 0.1	3.0 ± 0.2	3.2 ± 0.8
11	BD+231799	5.1 ± 0.4	1.2 ± 0.3	3.0 ± 0.3	3.1 ± 0.2
12	HO Cnc	5.6 ± 0.5	0.9 ± 0.2	3.8 ± 0.4	3.4 ± 0.2
13	HP Cnc	5.1 ± 0.4	1.0 ± 0.1	3.1 ± 0.2	2.7 ± 0.2
14	V402 Hya	5.1 ± 0.4	1.0 ± 0.1	3.0 ± 0.2	3.9 ± 0.1
15	V405 Hya	5.1 ± 0.4	1.0 ± 0.1	3.0 ± 0.2	3.1 ± 0.4
16	GT Leo	5.1 ± 0.4	1.0 ± 0.1	3.0 ± 0.2	2.7 ± 0.2
17	V417 Hya	5.1 ± 0.4	1.2 ± 0.3	3.1 ± 0.2	2.6 ± 0.0
18	LR Hya	5.1 ± 0.4	1.1 ± 0.1	3.0 ± 0.2	2.4 ± 0.5
19	V418 Hya	5.1 ± 0.4	1.0 ± 0.1	3.0 ± 0.2	2.3 ± 0.5
20	AB Crt	5.5 ± 0.6	1.2 ± 0.3	3.7 ± 0.4	3.6 ± 0.2
21	HL Leo	4.2 ± 0.2	1.0 ± 0.1	2.2 ± 0.0	3.0 ± 0.6
22	GQ Leo	5.6 ± 0.5	0.9 ± 0.1	3.8 ± 0.4	3.1 ± 0.4
23	PQ Vir	5.1 ± 0.4	1.0 ± 0.1	3.0 ± 0.2	2.4 ± 0.8
24	MY Uma	5.1 ± 0.4	1.0 ± 0.1	3.0 ± 0.2	2.4 ± 0.4
25	PR Vir	5.5 ± 0.6	1.0 ± 0.1	3.6 ± 0.4	3.2 ± 0.7
26	FZ Leo	4.3 ± 0.2	1.0 ± 0.0	2.4 ± 0.0	2.7 ± 0.3
27	LV Com	5.1 ± 0.4	1.0 ± 0.1	3.0 ± 0.2	2.6 ± 0.6
28	DO CVn	5.1 ± 0.4	1.2 ± 0.3	3.0 ± 0.3	3.2 ± 0.3
29	LX Com	5.1 ± 0.4	1.2 ± 0.3	3.0 ± 0.3	2.9 ± 0.3
30	PX Vir	5.1 ± 0.4	1.0 ± 0.1	3.0 ± 0.2	2.5 ± 0.2
31	GY Boo	5.1 ± 0.4	1.0 ± 0.1	2.7 ± 0.2	3.0 ± 0.6
32	GZ Boo	5.1 ± 0.4	1.0 ± 0.1	3.0 ± 0.2	3.0 ± 0.4
33	HO Boo	5.1 ± 0.4	1.0 ± 0.1	3.0 ± 0.2	3.5 ± 0.4
34	FN Boo	5.6 ± 0.4	0.6 ± 0.2	3.9 ± 0.4	4.7 ± 0.0
35	V1022 Her	5.6 ± 0.4	0.8 ± 0.2	3.8 ± 0.4	3.4 ± 0.2
36	V401 Vul	5.5 ± 0.6	0.9 ± 0.1	3.5 ± 0.4	4.1 ± 0.3
37	V402 Peg	5.1 ± 0.4	1.0 ± 0.1	3.0 ± 0.2	3.9 ± 0.4
38	OT Peg	5.1 ± 0.4	1.0 ± 0.1	3.0 ± 0.2	3.4 ± 0.3
39	V383 Lac	5.1 ± 0.4	1.0 ± 0.1	3.0 ± 0.2	2.4 ± 0.3
40	HD 218782	5.1 ± 0.4	1.0 ± 0.1	3.0 ± 0.2	3.6 ± 0.1

best-fitting straight lines. Similar to the P versus log (R'_{HK}) correlation, a positive correlation was found between P versus log(R_X). The correlation was also found to be wavelength dependent: strong in B band and weak in I band (see Table 3). The slopes of linear regression fit between these two quantities are found to be 0.059 $\pm$ 0.012, 0.029 $\pm$ 0.007, 0.020 $\pm$ 0.005 and 0.008 $\pm$ 0.004 in the B, V, R and I bands, respectively. Similar to other slopes for above derived correlations, the slopes of P and log(R_X) correlation was found to be steeper in B-band than that in V, R, and I bands.

5 DISCUSSION AND CONCLUSIONS

We have carried out the broad-band linear polarimetric observations of a sample of 43 active dwarfs. The degree of polarization in these stars are found to be decreasing towards longer wavelengths with average values of 0.16 $\pm$ 0.01, 0.080 $\pm$ 0.006, 0.056 $\pm$ 0.004 and 0.042 $\pm$ 0.003 per cent in B, V, R, and I photometric bands, respectively. This type of behaviour is similar to that which has also been observed in some other active stars (e.g. Huovelin et al. 1985; Huovelin, Saar & Tuominen 1988; Yudin & Evans 2002; Alekseev 2003; Rostopchina et al. 2007; Golovin et al. 2012; Patel et al. 2013). The observed polarizations in these active dwarfs are also comparable to that of another class of active stars, namely RS CVn binaries (see Liu & Tan 1987; Scalitriti et al. 1993). However, the intrinsic polarizations in a few active stars are found to be more than the average values of polarization in these active dwarfs. Polarization up to 0.6 per cent has been reported in some other active stars (e.g. Pfeiffer 1979; Pandey et al. 2009). We have investigated the origin of polarization in these stars and have found a variety of results. In three stars, namely V526 Aur, V1658 Aql and V1659 Aql, the polarization is due to the ISM. However, polarization in 40 stars was found to be intrinsic rather than ISM induced. In order to find the origin of polarization in these stars, we have compared the observed values of polarization with theoretically obtained values of polarization either due to magnetic intensification or due to scattering. It appears that the scattering alone is not responsible for the net polarization in these active dwarfs. In a few active stars, MI is found to be the sole origin of polarization. But in a majority of stars in the sample, the observed polarization is comparable to the sum of polarization due to MI plus scattering. This indicates that the net

polarizations in active dwarfs are due to the combined effect of MI and scattering. The wavelength dependence of polarization provides another test to distinguish the causes of polarization in late-type active stars whether it is due to magnetic intensification or due to scattering. In order to determine wavelength-dependence polarization, we have also fit the power law $P \propto \lambda^{-b}$ to the observed and theoretical values of polarization. The derived values of power-law indices 'b' for the observed polarization and the theoretical polarization are then compared. A similar analysis has also been done by Huovelin et al. (1985, 88) for the average values of polarization in U, B, V and R bands. The values of 'b' are given in Table 4, where $b_{\rm O}$, $b_{\rm M}$, $b_{\rm S}$ and $b_{\rm MS}$ are power-law index for observed, MI, scattering, and MI plus scattering polarization, respectively. Only for the star V538 Aur, the values of $b_{\rm M}$ and $b_{\rm O}$ were found to be well within 1σ level, indicating polarization to be purely magnetic in origin. While comparing $b_{\rm S}$ and $b_{\rm O}$, we found that $b_{\rm O}$ was well above the 2σ level from $b_{\rm S}$ for all the active dwarfs, which further shows that the polarization in these active dwarfs is not due to scattering. However, for most of active dwarfs, the values of $b_{\rm MS}$ was comparable with $b_{\rm O}$ within 1σ level. This again shows that in a majority of active dwarfs, the linear polarization was due to the sum of polarization due to MI and polarization due to scattering. There are a few stars, namely BD-04° 234, V1221 Tau, and V402 Hya, where $b_{\rm O}$ is well above the 3σ level than $b_{\rm MS}$, indicating the presence of supplementary sources of linear polarization (see Pfeiffer 1979; Pandey et al. 2009). The theoretical modelling of Saar & Huovelin (1993) showed that the magnetic field of 2–3 kG for K-type stars, 1.3–2 kG for G-type stars, and 0.5–1.2 kG for F-type stars are required to produce the polarization due to MI. In our sample, a majority of stars show the polarization due to MI; therefore, the magnetic field in the sample of stars could be in the range of 0.5–3.0 kG.

We have also studied the correlations between linear polarizations and magnetic activity indicators R_O, $R'_{\rm HK}$, and $R_{\rm X}$. It is found that the degree of polarization increases with increasing magnetic activity in late-type dwarfs. Huovelin et al. (1988) also found that the linear polarization is related with activity indicators, but in a complex way. The slopes of linear regression fit between P and R_O are found to be steeper than those derived by Huovelin et al. (1988) for nine other active dwarfs. All the correlations are found to be similar, which is expected as all the activity indicators are correlated with each other (Noyes et al. 1984; Randich 2000). These correlations are found to be strongest in the B band and also show the largest slope of linear regression fit in the B band. The correlation becomes weaker towards longer wavelengths. This could be due to the increase in the number of saturated Zeeman-sensitive absorption lines towards the blue end of the optical spectrum, which in turn produce net linear polarization via the magnetic intensification mechanism and scattering in the optically thin part of stellar atmosphere. The observed polarization is found to be $(B - V)$ colour dependent i.e. the redder the star, the larger is the observed polarization. This is consistent with a trend observed in the U band by Piirola (1977), Tinbergen & Zwaan (1981), Alekseev (2000) and in U, B, V bands by Huovelin et al. (1988). The observed wavelength dependences of linear polarizations and their trend with $(B - V)$ support the magnetic intensification mechanism as the dominant contributor to the observed polarization.

We conclude that the linear polarization in majority of active dwarfs are due the combined effect of magnetic intensification and scattering, where the degree of polarization is strongly correlated with various activity parameters, especially at the blue end of the optical electro-magnetic spectrum.

ACKNOWLEDGEMENTS

This work was done under the Indo-Russian DST-RFBR project reference INT/RUS/RFBR/P-167 (for India) and Grant RFBR Ind_a 14-02-92694 (for Russia). We thank the referee for reading the manuscript carefully and for his comments/suggestions. MKP thanks Dr C. Eswaraiah for useful discussion. SK acknowledges A. Joshi, S. Neha, and B. J. Medhi for their help in observations.

REFERENCES

Alekseev I. Y., 2000, Astron. Rep., 44, 696
Alekseev I. Y., 2003, Astron. Rep., 47, 430
Brown J. C., McLean I. S., 1977, A&A, 57, 141
Brown J. C., McLean I. S., Emslie A. G., 1978, A&A, 68, 415
Calamai G., Degl'Innocenti E. L., 1983, A&AS, 53, 311
Calamai G., Landi Degl'Innocenti E., Landi Degl'Innocenti M., 1975, A&A, 45, 297
Claret A., Bloemen S., 2011, A&A, 529, 75
Degl'Innocenti E. L., 1983, Sol. Phys., 85, 33
Dollfus A., 1958, C. R. Acad. Sci., Paris I, 246, 3590
Duncan D. K. et al., 1991, ApJS, 76, 383
Eswaraiah C., Pandey A. K., Maheswar G., Medhi B. J., Pandey J. C., Ojha D. K., Chen W. P., 2011, MNRAS, 411, 1418
Finn G. D., Jefferies J. T., 1974, Sol. Phys., 39, 91
Golovin A. et al., 2012, MNRAS, 421, 132
Huovelin J., Saar S. H., 1991, ApJ, 374, 319
Huovelin J., Linnaluoto S., Piirola V., Tuominen I., Virtanen H., 1985, A&A, 152, 357
Huovelin J., Saar S. H., Tuominen I., 1988, ApJ, 329, 882
Huovelin J., Linnaluoto S., Tuominen I., Virtanen H., 1989, A&AS, 78, 129
Kemp J. C., Wolstencroft R. D., 1974, MNRAS, 161, 1
Leroy J. L., 1962, Ann. Astrophys., 25, 127
Leroy J. L., Le Borgne J. F., 1989, A&A, 223, 336
Liu X.-f., Tan H.-S. Y., 1987, Chin. Astron. Astrophys., 11, 244
Medhi B. J., Maheswar G., Pandey J. C., Tamura M., Sagar R., 2010, MNRAS, 403, 1577
Middelkoop F., 1982, A&A, 107, 31
Mullan D. J., Bell R. A., 1976, ApJ, 204, 818
Noyes R. W., Hartmann L. W., Baliunas S. L., Duncan D. K., Vaughan A. H., 1984, ApJ, 279, 763
Orsatti A. M., Vega E., Marraco H. G., 1998, AJ, 116, 266
Pace G., 2013, A&A, 551, L8
Pandey J. C., Medhi Biman J., Sagar R., Pandey A. K., 2009, MNRAS, 396, 1004
Patel M. K., Pandey J. C., Savanov I. S., Prasad V., Srivastava D. C., 2013, MNRAS, 430, 2154
Pfeiffer R. J., 1979, ApJ, 232, 181
Piirola V., 1977, A&AS, 30, 213
Piirola V., Vilhu O., 1982, A&A, 110, 351
Randich S., 2000, in Pallavicini R., Micela G., Sciortino S., eds, ASP Conf. Ser. Vol. 198, Stellar Clusters and Associations: Convection, Rotation, and Dynamos. Astron. Soc. Pac., San Francisco, p. 401
Rautela B. S., Joshi G. C., Pandey J. C., 2004, Bull. Astron. Soc. India, 32, 159
Rostopchina A. N., Grinin V. P., Shakhovskoi D. N., Lomach A. A., Minikulov N. K., 2007, Astron. Rep., 51, 55
Rutten R., 1984, A&A, 130, 353
Saar S. H., Huovelin J., 1993, ApJ, 404, 739
Scalitriti F., Piirola V., Coyne G. V., Koch R. H., Elias N. M., Holenstein B. D., 1993, A&AS, 102, 343
Schmidt G. D., Elston R., Lupie O. L., 1992, AJ, 104, 1563
Serkowski K., 1970, ApJ, 160, 1083

Serkowski K., 1973, in Greenberg J. M., van de Hulst H. C., eds, Proc. IAU Symp. Vol. 52, Interstellar Dust and Related Topics. Kluwer, Dordrecht, p. 145
Serkowski K., Mathewson D. S., Ford V. L., 1975, ApJ, 196, 261
Soam A., Maheswar G., Eswaraiah C., 2014, Ap&SS, 350, 251
Tinbergen J., Zwaan C., 1981, A&A, 101, 223
Vaughan A. H., Preston G. W., 1980, PASP, 92, 385
Vaughan A. H., Preston G. W., Wilson O. C., 1978, PASP, 90, 267
Voges W. et al., 1999, A&A, 349, 389
Whittet D. C. B., van Breda I. G., 1978, A&A, 66, 57
Yudin R. V., Evans A., 2002, A&A, 386, 916

This paper has been typeset from a TEX/LATEX file prepared by the author.